nature communications

Article

https://doi.org/10.1038/s41467-025-67588-6

Dysfunctional CD4 T cells in an oncovirus-specific TCR-transgenic in vivo model

Received: 1 April 2025

Accepted: 4 December 2025

Published online: 18 December 2025

Check for updates

Felicia S. Spitzer[1], Marcel G. M. Camps[1], Cedrik M. Britten[1,2], Sandra Vloemans[1], Hester J. T. van Zeeburg[1], Cornelis J. M. Melief[1], Tsolere Arakelian[1] & Ferry Ossendorp[1]

T cell exhaustion has been implicated in cancer and infectious diseases. In this study, we report a novel mouse model, "MolT-II", with T cells expressing a transgenic T cell receptor (TCR) specific for a Moloney virus envelope-derived, MHC class II-presented peptide epitope. Characterization of MolT-II CD4 T cells revealed that they are dysfunctional, showing severely impaired effector functions, reduced proliferation and increased baseline expression of co-inhibitory receptors such as PD-1, LAG-3 and CTLA-4, likely due to chronic exposure to a self-antigen. We further show that epitope-specific peptide vaccination combined with immune checkpoint blockade is able to restore the function of MolT-II CD4 T cells in vivo, associated with enhanced tumor control in mice. The MolT-II mouse strain thus represents an in vivo model for reversible CD4 T cell dysfunction, allowing the study of the role of CD4 T cell regulation in cancer, mechanisms underlying CD4 T cell dysfunction and exhaustion, and novel immunomodulatory therapies aiming to rescue dysfunctional T cells.

Prolonged antigen exposure can lead to tolerization and dysfunction of antigen-specific T cells. Such T cell "exhaustion" can occur in the context of chronic infection or growing tumors[1–4]. While CD8 T cell exhaustion is being studied extensively and many treatments currently in use aim to rehabilitate dysfunctional CD8 T cells, the role of exhaustion or dysfunction of CD4 T cells remains largely understudied, despite their central role in different immune processes[5]. In cancer, CD4 T cells have been shown to take on a myriad of roles, most important of which is providing help to CD8 T cells for the mounting and maintenance of an effective anti-tumor response[6]. Further, CD4 T cells can suppress immune responses as regulatory CD4 T cells (Tregs)[7,8]. Also, CD4 T cells can engage in tumor eradication through direct cytotoxicity[9,10] or interaction with other immune cells such as macrophages[11–13]. Extensive multidimensional analysis of thousands of human solid tumors has shown the presence of both CD4 and CD8 T cells in the tumor microenvironment correlating with immunotherapy efficacy by blocking coinhibitory receptors like PD-1. This indicated dysfunctional states of immune cell clusters in many types of cancer[14–16].

T cell dysfunction comes in several flavors which can differ in cause; however, most are characterized by reduced proliferative activity, expression of co-inhibitory markers, downregulation of the TCR signaling machinery and abnormal cytokine expression[17–19].

In cancer, T cell exhaustion has been extensively researched, especially in relation to immunotherapy, with a primary focus on CD8 T cells. Chronic antigen exposure is thought to be one of the main causes underlying T cell exhaustion[3,20,21], and recent studies suggest that dysfunctional states similar to those found in CD8 T cells can also be observed in different CD4 T cell populations, and may indeed be clinically relevant[5,22]. Several cancer immunotherapies target molecules associated with T cell exhaustion like PD-1, LAG-3 and CTLA-4 in order to reinvigorate T cell function[23–25]. And while immune checkpoint inhibition is an effective therapeutic option, the high rate of non-responders and the unwanted side effects leave room for improvement[2,26,27].

We generated a T cell receptor (TCR)-transgenic mouse model named "MolT-II" (in analogy to the OT-II mouse strain) to investigate

[1]Department of Immunology, Leiden University Medical Center, Leiden, The Netherlands. [2]Present address: Immatics Biotechnologies, Munich, Germany. e-mail: f.a.ossendorp@lumc.nl

tumor-specific CD4 T cell responses to murine leukemia virus (MuLV)-induced cancers. The Friend, Moloney, and Rauscher ("FMR") virus types are well-characterized exogenous MuLVs that can induce leukemias, lymphomas and sarcomas in mice[28]. Several virus-derived CD4 and CD8 T cell epitopes have been shown to play critical roles in the immune response against these tumors[29,30]. Most importantly, previous research has shown that CD4 T cells directed against an I-A^b-presented peptide epitope derived from the Moloney virus envelope protein are by themselves sufficient to protect against virus-induced sarcoma lesions and enhance tumor-specific CD8 T cell responses against MHC class II-negative lymphoma cells[29,31].

In this report we describe the TCR-transgenic MolT-II mouse strain, whose CD4 T cells show a dysfunctional phenotype characterized by severely diminished proliferation, lack of cytokine secretion, upregulation of co-inhibitory checkpoint molecules and inadequate response to antigen-specific TCR stimuli. This phenotype appears to be driven by cross-reactivity between the transgenic TCR and the common endogenous murine retrovirus AKV (originally found in AKR mice). Rescue of MolT-II CD4 T cell function can be achieved through antigen-specific TCR stimulation and combined blockade of co-inhibitory checkpoint molecules PD-1, CTLA-4 and LAG-3, and functionally reinvigorated MolT-II CD4 T cells can contribute to tumor control in mice bearing MuLV-induced lymphoma

This new mouse model mirrors the phenotype of exhausted CD4 T cells found in cancer, infections and autoimmune diseases, enabling the study of mechanisms underlying T cell dysfunction and how to reinvigorate T cells.

Results

Reduced CD4 T cell compartment in TCR-transgenic MolT-II mice

The newly generated TCR-transgenic MolT-II mice, expressing the TCRα and β chains derived from a CD4 T cell clone specific for Moloney MuLV env-gp70 peptide sequence 119-137 (envH), bred normally and did not present with any obvious phenotypic aberrations. The majority of peripheral CD4 T cells of MolT-II mice expressed the TCR-transgenic Vβ6 chain, comparable to the expression of the transgenic Vβ5 chain in OT-II mice, another model for transgenic CD4 T cells specific for chicken ovalbumin peptide sequence 323-339 (ovaH) (Fig. 1A). Analysis of the lymphoid system revealed an unusually low frequency of CD4 T cells in the spleens, lymph nodes and blood of MolT-II mice (Fig. 1B). Wild type C57BL/6 mice had a CD8:CD4 T cell ratio with ranges between 0.5:1 and 0.7:1, while the CD8:CD4 ratio in OT-II mice ranged between 0.2:1 and 0.5:1, likely due to positive selection of the TCR-transgenic CD4 T cells in the thymus and lack of negative selection of the ovalbumin-specific TCR. Unexpectedly, in MolT-II mice, we found the CD8:CD4 ratio to be drastically increased to around 1.7:1 in secondary lymphoid organs and blood (Fig. 1C). We further found that the total number of CD3-positive T cells was comparable between the different mouse strains (Fig. 1D), but the number of CD4 T cells in MolT-II spleens was significantly lower than in C57BL/6 and OT-II mice (Fig. 1E). Thus, the CD4 T cells of MolT-II mouse express the transgenic TCR, but the frequency of these CD4 T cells in the periphery is significantly reduced.

MolT-II CD4 T cells show decreased effector functions in response to peptide stimulation

After assessing the diminished cellularity of the CD4 T cell compartment of MolT-II mice, we analyzed the functionality of the CD4 T cells. CD4 T cells from MolT-II and OT-II mice were stimulated by co-culturing splenocytes with envH or ovaH peptide-loaded dendritic cells (DCs) (Figs. 2A, B). While MolT-II CD4 T cells were able to express moderate levels of CD40L, IL-2 and TNF, the magnitude of the response was significantly lower than OT-II CD4 T cells stimulated with their cognate epitope (ovaH), which induced very high expression of CD40L and TNF, as well as increased IL-2 expression.

Further, we tested the proliferative capacities of TCR-transgenic MolT-II and OT-II CD4 T cells after stimulation with envH or ovaH peptide, respectively. To that end, CFSE-labeled splenocytes were incubated with peptide-loaded DCs for 96 h, followed by flow cytometric analysis (Fig. 2C). For OT-II CD4 T cells, even low concentrations of ovaH peptide induced strong proliferation, as shown by the high proportion of divided $CFSE^{low}$ CD4 T cells. In contrast, stimulation of MolT-II CD4 T cells with envH peptide induced proliferation only to a low extent, even at high peptide concentrations.

The lack of cytokine expression and reduced proliferative capacity showed that MolT-II CD4 T cells are unable to appropriately respond to stimulation with MHC class II-presented envH peptide. This could be caused by low avidity between MolT-II TCR and the peptide-MHC complex (pMHC) or insufficient interaction time between TCR and pMHC[32,33]. To assess whether a more potent stimulus would be able to trigger the transgenic MolT-II TCR and lead to an improved cytokine response, C57BL/6, MolT-II and OT-II splenocytes were stimulated with 1 μg/ml each of soluble αCD3 (Signal 1) and soluble αCD28 (Signal 2) (Fig. 2D). Stimulation with these soluble antibodies led to high expression of CD40L, IL-2 and TNF by CD4 T cells from all three mouse strains. In response to the stimulation, MolT-II CD4 T cells produced IL-2 to even higher levels than wild type and OT-II CD4 T cells. These results, indicating regained function by high affinity co-stimulation, show that the low responses observed after envH stimulation do not reflect irreversible dysfunction of MolT-II CD4 T cells.

Expression of co-inhibitory checkpoint molecules is indicative of CD4 T cell dysfunction

Immune regulatory signaling may be involved in the dysfunctional phenotype of CD4 T cells in MolT-II mice. First, we found that MolT-II mice harbor a similar frequency of Tregs (regulatory T cells, $FoxP3^+CD25^+CD4^+$) compared to wild type mice (Supplementary Fig. 1A). Rather, we found that the number of Tregs in spleens from OT-II mice was lower than in the other two mouse strains.

This suggested that the functional deficits observed in MolT-II CD4 T cells might be due to intrinsic regulatory pathways in the T cells themselves. Flow cytometric analysis of CD4 T cells from naive MolT-II, C57BL/6 and OT-II mice showed that several co-inhibitory immune checkpoint molecules, such as PD-1, LAG-3, CTLA-4, and TIM-3 were upregulated on MolT-II CD4 T cells (Fig. 2E, Supplementary Fig. 2A). We also observed higher expression of co-stimulatory checkpoint molecules ICOS and OX40 on MolT-II CD4 T cells (Supplementary Fig. 2B, C), which has been previously described to occur in exhausted CD4 but not CD8 T cells[34].

Stimulation of the cells with αCD3 antibody, without CD28 co-stimulation, using low (200 ng/ml) or high dose conditions (1 μg/ml) further increased the expression of checkpoint molecules, far beyond the expression levels of C57BL/6 and OT-II CD4 T cells (Fig. 2E). On the other hand, stimulation of MolT-II CD4 T cells with peptide envH had no notable effects on the expression of checkpoint molecules (Supplementary Fig. 2D).

Taken together, the high expression of co-inhibitory molecules, lack of cytokine production in response to cognate antigen encounter and limited proliferative capabilities suggest that MolT-II CD4 T cells are in a state of functional exhaustion.

MolT-II CD4 T cells recognize a cross-reactive endogenous peptide ligand

Upon investigation of splenic CD4 T cells we noticed that the MolT-II CD4 T cell population had a significantly smaller proportion of $CD62L^+CD44^-$ CD4 T cells compared to C57BL/6 and OT-II (Fig. 3A, Supplementary Fig. 3A, B). Furthermore, a larger percentage of CD4

https://doi.org/10.1038/s41467-025-67588-6

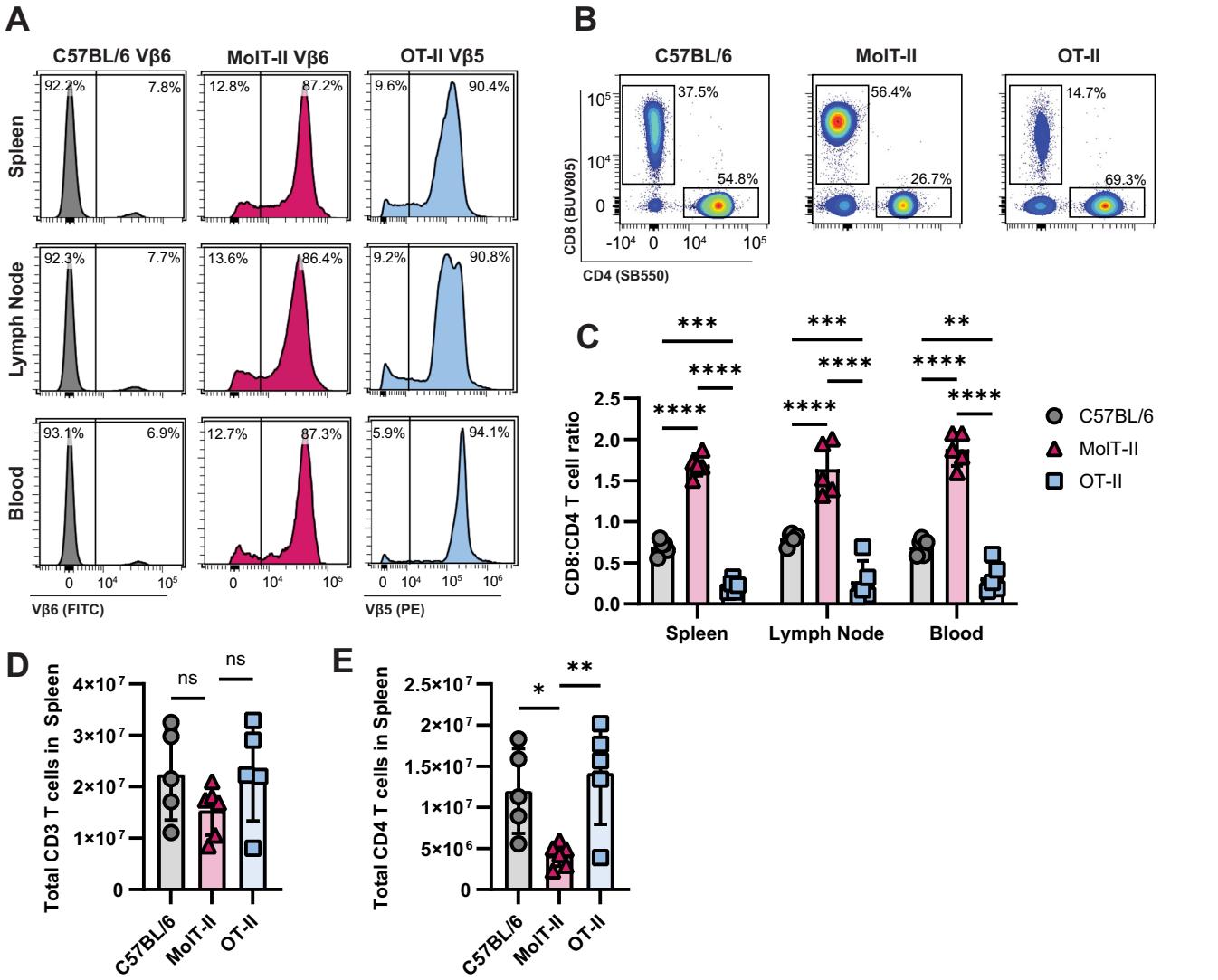

Fig. 1 | Characterization of CD4 T cell population in the MolT-II mouse strain. **A** Expression of the transgenic TCR Vβ6 chain on MolT-II CD4 T cells, compared to the expression of Vβ6 on wild type C57BL/6 CD4 T cells and the expression of the transgenic TCR Vβ5 chain on OT-II CD4 T cells, on cells from the spleen, lymph nodes and blood. **B** Representative dot plots from flow cytometric analysis of C57BL/6, MolT-II, and OT-II splenocytes stained for CD8 (Y axis) and CD4 (X axis). **C** Ratio of CD8 T cells to CD4 T cells in lymph nodes, spleens and blood of C57BL/6, MolT-II and OT-II mice (n = 5 per mouse strain; exact p-values can be found in the Source Data file). **D** Analysis of the total numbers of CD3 T cells and **E** CD4 T cells in the spleens of C57BL/6 (n = 5), MolT-II (n = 6) and OT-II mice (n = 5; C57BL/6 vs. MolT-II p = 0.0376, MolT-II vs. OT-II p = 0.0087). Bar graphs show mean and SD, statistical significance (* $p \le 0.05$; ** $p \le 0.01$; *** $p \le 0.001$; **** $p \le 0.0001$; or ns for not significant) was determined by one-way ANOVA followed by Tukey's multiple comparisons test for (D) and (E), and by two-way ANOVA and Tukey's multiple comparisons test for (**C**).

T cells were CD44 positive ($CD44^+CD62L^-$ and $CD44^+CD62L^+$), which is uncharacteristic of naive mice. CD44 is considered a marker for T cell activation, effector and memory T cells and therefore antigen-experience[35]. The high expression of CD44 might be due to interactions between MolT-II CD4 T cells and an endogenous peptide ligand underlying the exhausted phenotype found in MolT-II T cells. Furthermore, cross-reactivity to an endogenous peptide ligand could lead to selective self-pressure, explaining the relatively low numbers of peripheral CD4 T cells in MolT-II mice. Investigation of thymocytes indicated that negative selection of the TCR-transgenic MolT-II CD4 T cells is not restricted to the periphery. The percentage of CD44-positive, antigen-experienced CD4 T cells in the thymus of MolT-II mice was significantly elevated compared to OT-II and C57BL/6 thymocytes (Supplementary Fig. 3C). Further, MolT-II mice showed a decreased proportion of $CD4^+CD8^+$ double-positive thymocytes compared to other mouse strains (Fig. 3B, Supplementary Fig. 3D), resembling findings in other TCR-transgenic mouse strains in which TCR ligands are expressed in the thymus inducing negative selection of self-reactive T cells[36,37]. As these results suggest the existence of a cross-reactive peptide ligand for the TCR-transgenic MolT-II CD4 T cells, we compared the sequence of the envH epitope to sequences from the mouse genome. This led to the discovery of a highly homologous sequence derived from the envelope protein of the endogenous murine retrovirus AKV ($env_{138\text{-}156}$, "AKVenv"). The sequences of the endogenous peptide AKVenv and the exogenous Moloney MuLV-derived peptide envH only differ in one amino acid ($envH_{124}$, $AKVenv_{143}$), where a leucine is replaced by a tyrosine in AKVenv (Fig. 3C). In order to analyze whether this sequence was expressed in the thymus of MolT-II mice, thymic stromal cells were isolated and sorted into different subsets (cortical thymic epithelial cells (cTECs), medullary thymic epithelial cells (mTECs) and thymic dendritic cells (DCs)) and analyzed by qPCR, using the thymoma cell line EL-4 as a positive control (Fig. 3D). These experiments demonstrate that AKVenv expression in the thymus is largely restricted to mTECs,

https://doi.org/10.1038/s41467-025-67588-6

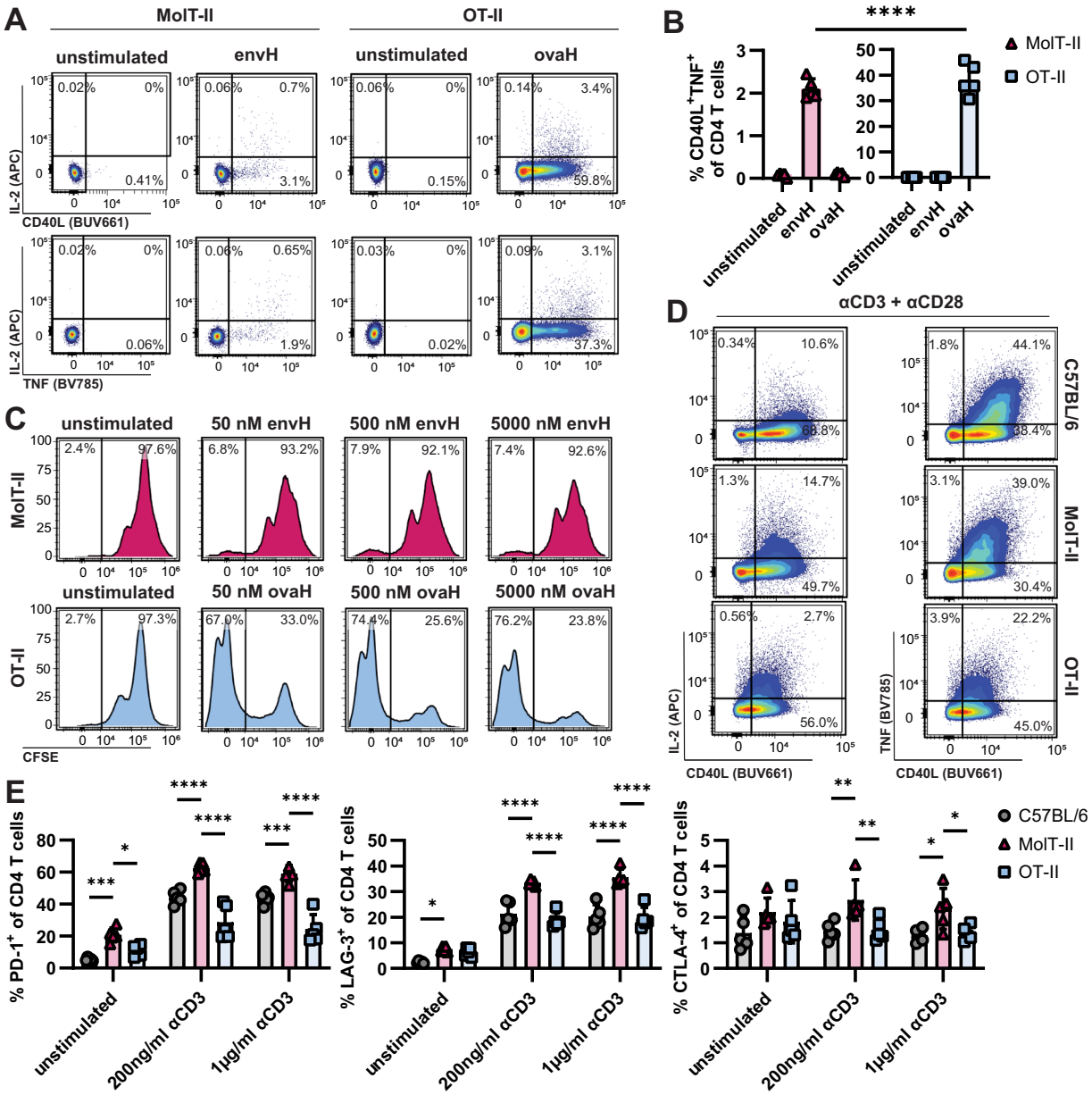

Fig. 2 | MolT-II CD4 T cells are dysfunctional and show characteristics of exhausted T cells. A Representative dot plots showing the expression of IL-2, CD40L and TNF by splenic CD4 T cells from MolT-II (n = 5) and OT-II mice (n = 5), co-cultured with D1 dendritic cells loaded with either no antigen (unstimulated) or with specific peptide ligands envH and ovaH. **B** Frequency of $CD40L^+TNF^+$ CD4 T cells from MolT-II and OT-II mice (n = 5 mice per strain) after stimulation with envH, ovaH or no antigen (unstimulated; MolT-II envH vs. OT-II ovaH $p < 0.0001$). **C** Representative histograms showing CFSE-labeled splenocytes from MolT-II and OT-II without stimulation or after stimulation with increasing concentrations (unstimulated, 50 nM, 500 nM, 5000 nM) of peptides envH and ovaH, respectively. **D** Dot plots showing the expression of CD40L, IL-2 and TNF by C57BL/6, MolT-II and OT-II CD4 T cells after in vitro stimulation with soluble αCD3e and αCD28 antibodies. **E** Expression of co-inhibitory checkpoint molecules PD-1, LAG-3 and CTLA-4 on CD4 T cells from C57BL/6, MolT-II and OT-II mice following either no stimulation, stimulation with suboptimal (200 ng/ml) or optimal (1 mg/ml) amounts of αCD3e (n = 5 per strain; exact p-values can be found in the Source Data file). Bar graphs show mean and SD, statistical significance (* $p \le 0.05$; ** $p \le 0.01$; *** $p \le 0.001$; **** $p \le 0.0001$; or ns for not significant) was determined by two-way ANOVA with Tukey's multiple comparisons test (E) or two-way ANOVA with Šídák's multiple comparisons test (B).

supporting their role in shaping central tolerance by mediating the deletion of autoreactive $CD4^+CD8^+$ thymocytes[38]. Expression of AKVenv was not detectable in cTECs and only low expression was found in thymic DCs.

Based on these findings, we further analyzed possible cross-reactivity of MolT-II CD4 T cells with the AKVenv epitope. CFSE-labeled MolT-II splenocytes were co-cultured for 96 h with DCs loaded with envH, AKVenv, or control peptide ovaH. Results showed that the AKVenv peptide was able to induce proliferation of MolT-II CD4 T cells, similar to, but at a lower level than envH stimulation (Fig. 3E), indicating cross-reactivity of the MolT-II TCR with the endogenous AKVenv peptide ligand. To further assess cross-reactivity of MolT-II cells with the endogenous AKVenv sequence, LPS-matured dendritic cells were loaded with envH, AKVenv, or control peptide ovaH and co-incubated over night with MolT-II splenocytes. Analysis of the MolT-II CD4 T cells by flow cytometry revealed that stimulation with AKVenv resulted in elevated expression of CD40L and TNF compared to the controls (Fig. 3F), but still

https://doi.org/10.1038/s41467-025-67588-6

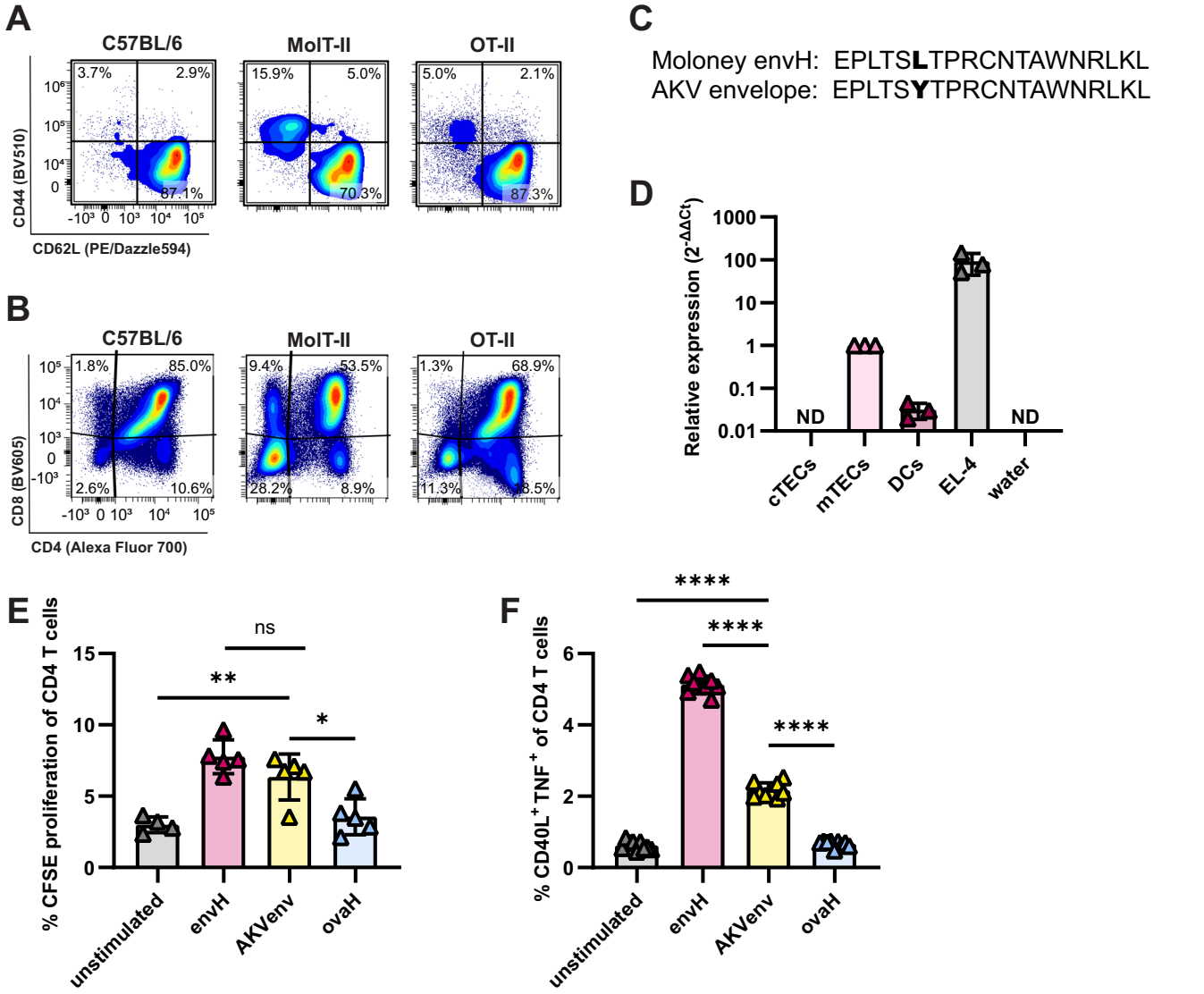

Fig. 3 | Cross-reactivity to an endogenous retrovirus epitope leads to negative selection of MolT-II CD4 T cells in the thymus. A Expression of CD62L and CD44 on CD4 T cells from the spleens of C57BL/6, OT-II, and MolT-II mice. Representative dot plots showing the data from n = 5 per strain. **B** Representative dot plots from flow cytometric analysis of mouse thymocytes. Plots show the expression of CD4 (X axis) and CD8 (Y axis) on thymocytes from C57BL/6, OT-II and MolT-II mice (n = 5 per strain). **C** Comparison of the amino acid sequences of the exogenous Moloney MuLV-derived envH$_{119\text{-}137}$ epitope and the envelope protein of the endogenous retrovirus AKV (epitope AKVenv$_{138\text{-}156}$). **D** Expression of AKV transcripts encoding the AKVenv epitope in thymic stromal cell subpopulations relative to the expression of beta actin and normalized to mTECs, as determined by quantitative PCR. qPCR was performed for AKVenv and housekeeping gene beta actin on flow-sorted cortical thymic epithelial cells (cTECs), medullary thymic epithelial cells (mTECs), CD11c$^+$F4/80$^-$ thymic dendritic cells (DCs) as well as the EL-4 thymoma cell line (positive control) and water (negative control). Columns show the relative expression ($2^{-\Delta\Delta Ct}$) of AKVenv, ND = not detected, data pooled from n = 3 independent experiments. **E** Proliferation of MolT-II CD4 T cells without stimulation or after stimulation with peptides envH, AKVenv or ovaH. Proliferation is shown as percent CFSE-negative CD4 T cells (n = 4 for 'unstimulated', n = 5 for 'envH', 'AKVenv' and 'ovaH'; unstimulated vs. AKVenv p = 0.0056, AKVenv vs. ovaH p = 0.0142, envH vs. AKVenv p = 0.3078). **F** Frequency of CD40L$^+$TNF$^+$ MolT-II CD4 T cells after co-incubation with mature D1 cells loaded with peptides envH, AKVenv, ovaH or without peptide (unstimulated, n = 9 per group, representative of 3 independent experiments; unstimulated vs. AKVenv p < 0.0001, envH vs. AKVenv p < 0.0001, AKVenv vs. ovaH p < 0.0001). Graphs show mean and SD, statistical significance (* p ≤ 0.05; ** p ≤ 0.01; *** p ≤ 0.001; **** p ≤ 0.0001; or ns for not significant) was determined by one-way ANOVA and Tukey's multiple comparisons test (E, F).

significantly lower than stimulation with envH. Similarly, AKVenv stimulation also led to increased expression of IL-2, CD25 and, to a lesser degree, CD69 (Supplementary Fig. 3E). Together, these findings indicate that MolT-II CD4 T cells are, albeit weakly, cross-reactive to AKVenv.

Dysfunction of MolT-II CD4 T cells in vivo

Our ex vivo experiments revealed that despite adequate expression of the transgenic TCR Vβ6 chain on MolT-II CD4 T cells, only a minor fraction of cells responded to stimulation with the cognate peptide epitope envH. Based on this, we investigated whether the functionally impaired CD4 T cells could be activated in vivo.

To analyze the in vivo responsiveness of MolT-II CD4 T cells we made use of the dual-color bioluminescence T cell reporter mouse strain "TbiLuc", which enables in vivo imaging of the localization and activation of T cells[39]. MolT-II and OT-II mice were crossbred to TbiLuc reporter mice to obtain F1 mice with luciferase-expressing TCR-transgenic CD4 T cells. These CD4 T cells, enriched from the

https://doi.org/10.1038/s41467-025-67588-6

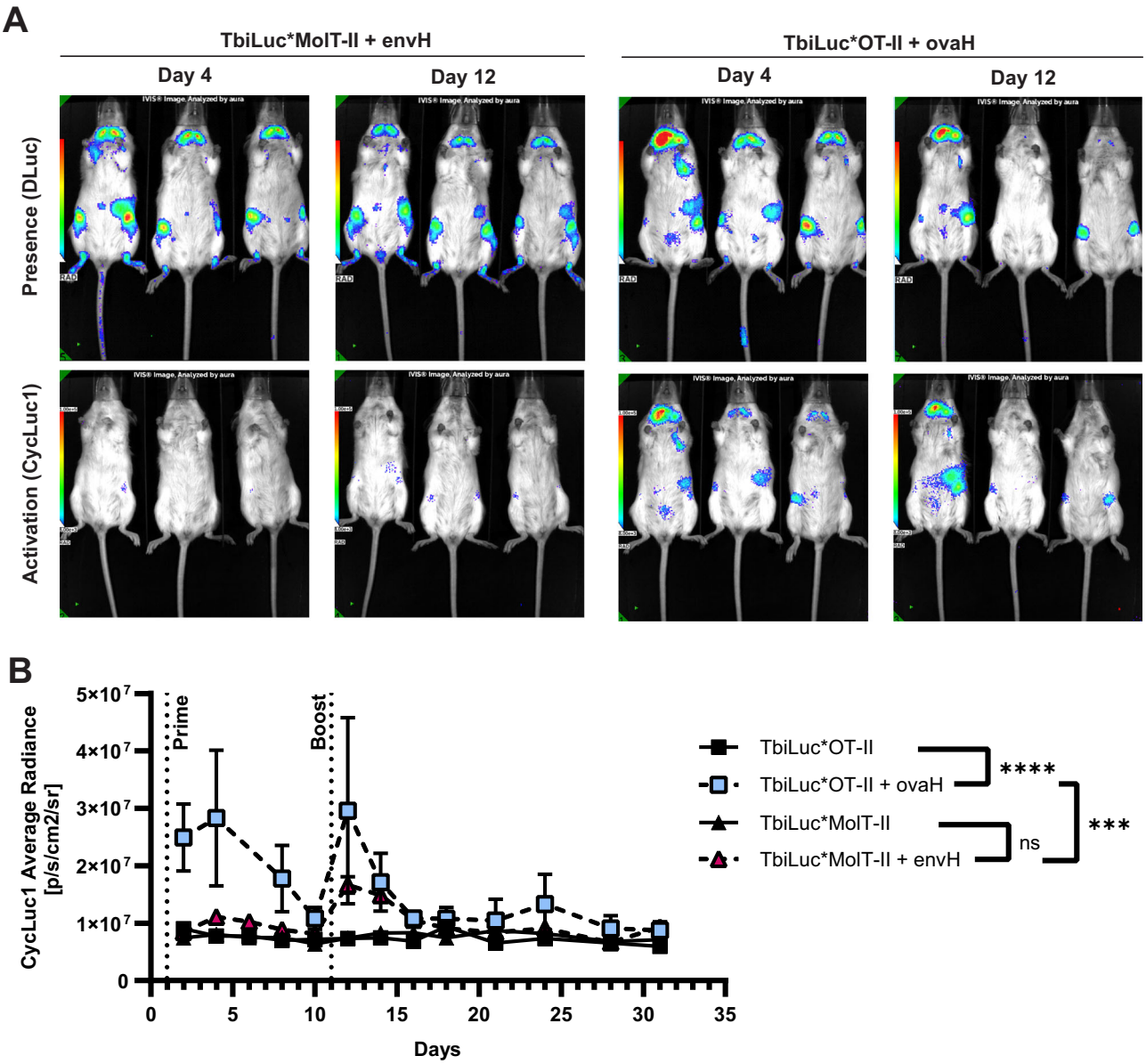

Fig. 4 | MolT-II CD4 T cells dysfunction persists in vivo after vaccination. **A** TbiLuc*MolT-II and TbiLuc*OT-II CD4 T cells were adoptively transferred into naive C57BL/6 wild type mice (day 0), followed by immunization with either envH + CpG or ovaH + CpG on days 1 and 11, or no treatment. Images show bioluminescence signals of CBG99/DLuc, indicating the presence of transferred TbiLuc T cells, and of PpyRE9/CycLuc1, indicating activation of TbiLuc T cells on days 4 and 12. **B** Bioluminescence signal (average radiance) after processing of the luciferase substrate CycLuc1 indicates the activation of the transferred CD4 T cells (n = 3 per group, representative of 2 independent experiments, graph shows mean and SEM over time; TbiLuc*MolT-II vs. TbiLuc*MolT-II + envH p = 0.2530, TbiLuc*OT-II vs. TbiLuc*OT-II + ovaH $p < 0.0001$, TbiLuc*MolT-II + envH vs. TbiLuc*OT-II + ovaH p = 0.0002). Statistical significance (* $p \le 0.05$; ** $p \le 0.01$; *** $p \le 0.001$; **** $p \le 0.0001$; or ns for not significant) was determined by two-way ANOVA and Tukey's multiple comparisons test.

spleens of naive TbiLuc*MolT-II or TbiLuc*OT-II mice, were adoptively transferred to naive C57BL/6 mice to enable accurate bioluminescence imaging and minimize background. After the T cell transfer, the recipient mice were vaccinated twice with envH + CpG (TbiLuc*MolT-II) or ovaH + CpG (TbiLuc*OT-II). Presence of the transferred cells in recipient mice was visualized by a click-beetle luciferase (CBG99), which is constitutively expressed by TbiLuc T cells, and luciferase substrate D-luciferin (Fig. 4A, upper). Upon activation, NFAT (Nuclear Factor of Activated T cells)-driven expression of a firefly luciferase (PpyRE9) enables the imaging of activated T cells with the substrate CycLuc1 (Fig. 4A, lower). Quantification of the average radiance of the CycLuc1 bioluminescence signal showed that vaccination with ovaH + CpG induced significant activation of TbiLuc*OT-II CD4 T cells compared to naive TbiLuc*OT-II CD4 T cells. (Fig. 4B). In contrast, envH + CpG vaccination only slightly increased the activation of TbiLuc*MolT-II CD4 T cells, further showing that MolT-II CD4 T cells are poorly responsive to antigenic stimulation in vivo.

Dysfunctional CD4 T cells can recover function after in vivo vaccination and immune checkpoint blockade

Based on the upregulation of immune checkpoint molecules on MolT-II CD4 T cells we had previously observed (Fig. 2D), we combined peptide vaccination with systemic blockade of the LAG-3, PD-1 and/or CTLA-4 pathways in vivo, aiming to restore T cell function (Fig. 5A). Systemic treatment with αLAG-3, αPD-L1 and αCTLA-4 had no effect on

https://doi.org/10.1038/s41467-025-67588-6

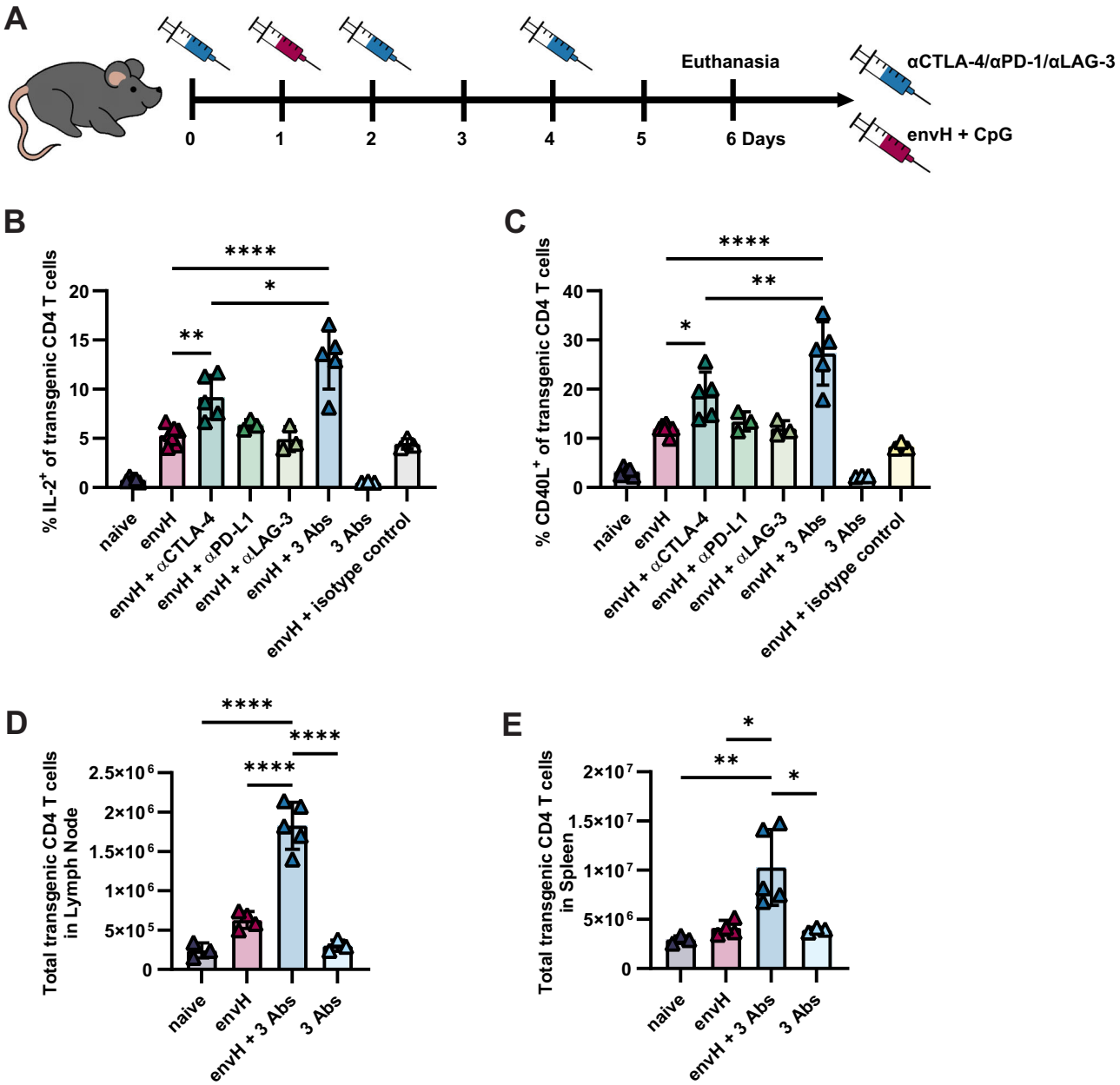

Fig. 5 | MolT-II CD4 T cells regain function after in vivo checkpoint blockade. **A** Treatment schedule indicating the intraperitoneal injection of checkpoint blocking antibodies αPD-L1, αLAG-3 and/or αCTLA-4 (200 μg each per dose) on days 0, 2, and 4, as well as intradermal vaccination with peptide envH (a cysteine-modified version of envH peptide to avoid oxidation) and adjuvant CpG on day 1, and sacrifice on day 6. **B** Lymph nodes of mice were collected on day 6 after starting treatment, and dysfunctional MolT-II CD4 T cells regained function, indicated by IL-2 (envH vs. envH + αCTLA-4 $p = 0.0079$, envH vs. envH + 3 Abs $p < 0.0001$, envH + αCTLA-4 vs. envH + 3 Abs $p = 0.0145$) and **C** CD40L expression (envH vs. envH + αCTLA-4 $p = 0.0289$, envH vs. envH + 3 Abs $p < 0.0001$, envH + αCTLA-4 vs. envH + 3 Abs $p = 0.0074$) in response to restimulation with envH, after treatment (n = 3-7 per group). **D** Absolute numbers of transgenic Vβ6+ CD4 T cells in the inguinal lymph nodes (naïve vs. envH + 3 Abs $p < 0.0001$, envH vs. envH + 3 Abs $p < 0.0001$, envH + 3 Abs vs. 3 Abs $p < 0.0001$) and **E** spleens (naïve vs. envH + 3 Abs $p = 0.0107$, envH vs. envH + 3 Abs $p = 0.0081$, envH + 3 Abs vs. 3 Abs $p = 0.0109$) of MolT-II mice (n = 3 for 'naïve' and '3 Abs', n = 3 for 'envH', n = 5 for 'envH + 3 Abs') after treatment with PBS (control), envH + CpG, triple antibody checkpoint blockade (αPD-L1 + αLAG-3 + αCTLA-4; "3 Abs"), or vaccination and triple checkpoint blockade. Graphs show mean and SD, statistical significance (* $p \le 0.05$; ** $p \le 0.01$; *** $p \le 0.001$; **** $p \le 0.0001$; or ns for not significant) was determined by one-way ANOVA and Tukey's multiple comparisons test (B, C, D, E).

the functional capabilities of MolT-II CD4 T cells (Fig. 5B, C). Vaccination with envH + CpG only slightly increased IL-2 and CD40L expression by MolT-II CD4 T cells. Combining vaccination with αLAG-3 or αPD-L1 had no significant additive effects. CTLA-4 blockade and vaccination could partly restore T cells function, however, simultaneous blockade of LAG-3, PD-L1 and CTLA-4 and vaccination led to a significant increase of IL-2+ and CD40L+ CD4 T cells. In addition, the absolute number of Vβ6+ CD4 T cells in the vaccine-draining lymph node and spleen of MolT-II mice significantly expanded in response to envH + CpG vaccination and triple checkpoint inhibition (Fig. 5D, E). Notably, treatment with triple checkpoint blockade alone had no effects on T cell function in naive MolT-II mice and required antigenic stimulation to take effect. This suggests that the presence of the endogenous peptide ligand AKVenv was not sufficient to overcome the tolerizing environment in vivo that restrains the CD4 T cells in a dysfunctional state.

https://doi.org/10.1038/s41467-025-67588-6

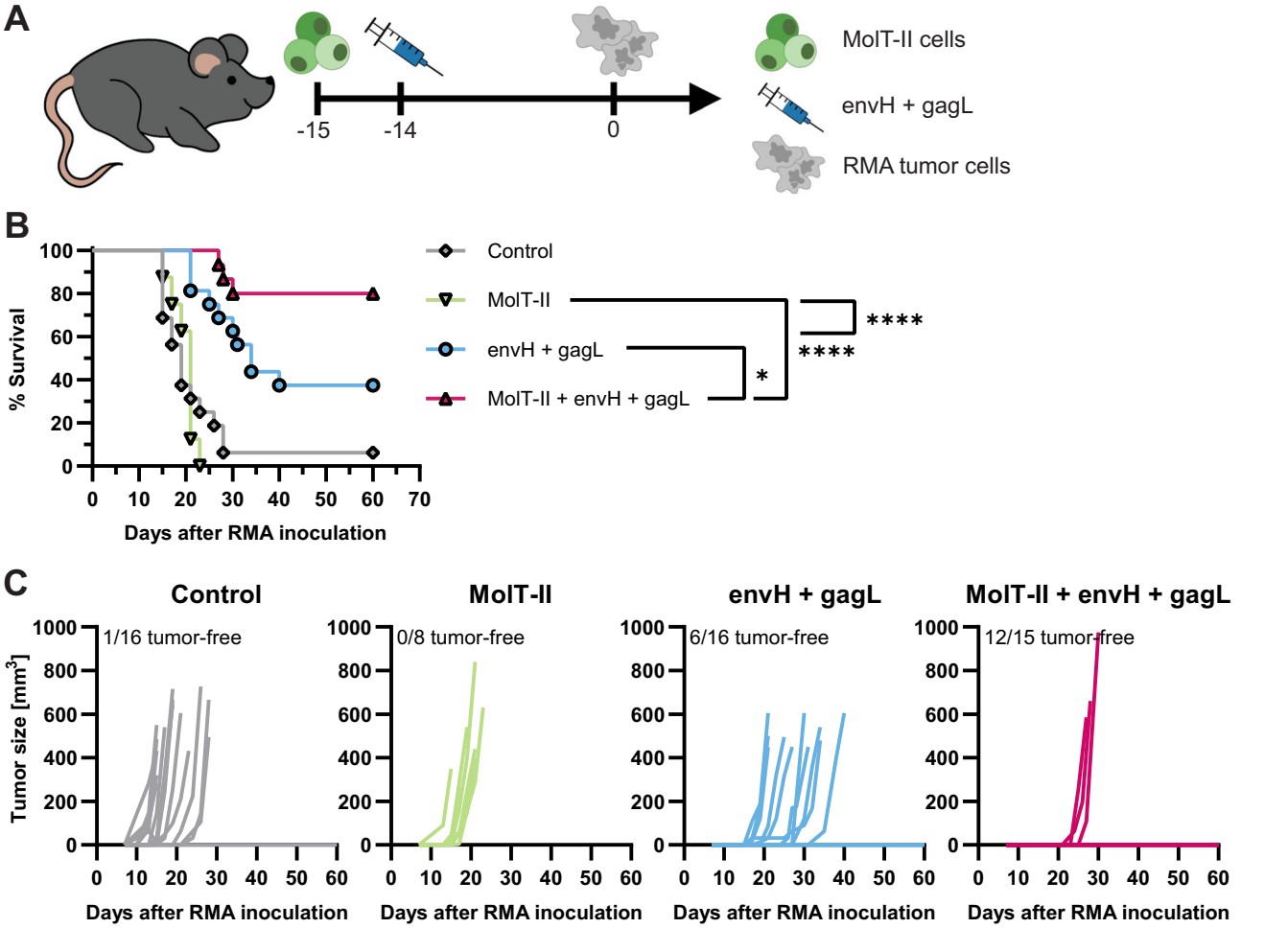

Fig. 6 | Recovered MolT-II T cells can control tumor growth in vivo. A Depending on the experimental group, C57BL/6 mice received a transfer of $1x10^7$ MolT-II cells on day -15, followed by vaccination with the helper epitope envH, combined with the dominant CTL epitope gagL emulsified in IFA (or only IFA) on day -14, and then subcutaneous injection with $2×10^3$ RMA tumor cells. **B** Graph shows the survival of RMA tumor-bearing mice that received control treatment (IFA only, n = 16), a transfer of MolT-II cells (n = 8), vaccination with envH + gagL (n = 16), or vaccination with envH + gagL and transfer of MolT-II cells (n = 15), (data pooled from two independent experiments, statistical significance was determined by Log-rank test; $p \le 0.05$; ** $p \le 0.01$; *** $p \le 0.001$; **** $p \le 0.0001$; MolT-II vs. envH + gagL $p < 0.0001$, MolT-II vs. MolT-II + envH + gagL $p < 0.0001$, envH + gagL vs. MolT-II + envH + gagL $p = 0.0209$). **C** Graphs showing the outgrowth of RMA tumors among the different groups over time.

MolT-II T cells can support tumor control in vivo upon robust vaccination

As we observed that MolT-II CD4 T cells were able to functionally recover in vivo, we evaluated whether MolT-II CD4 T cells were also able to contribute to tumor control. To that end we transferred MolT-II cells into naïve C57BL/6 mice. The next day, these recipient mice received a peptide vaccine consisting of envH combined with the dominant MuLV CTL epitope "gagL", emulsified in incomplete Freund's adjuvant (IFA). This formulation has shown to be effective in CD8-mediated tumor control in a previous study[29]. The mice were stratified into four groups receiving either IFA (Control), vaccination (envH + gagL), adoptive transfer of MolT-II cells (MolT-II), or a combination of vaccination and adoptive MolT-II cell transfer (MolT-II + envH + gagL). Two weeks later, the animals were all subcutaneously injected with a lethal dose of RMA tumor cells (Fig. 6A). Treatment with IFA or with MolT-II cells only did not contribute to tumor control (Fig. 6B). Vaccination with envH and gagL delayed the outgrowth of RMA tumors, and protected about 40 % of mice. Combining the vaccination with the transfer of MolT-II cells significantly increased the survival of mice to 80% (Figs. 6B, C). These findings indicate that after transfer, MolT-II CD4 T cells can regain functional helper activity when properly activated by robust peptide vaccination, to enhance CD8 T cell-mediated tumor control in vivo.

Discussion

In this study we present a novel transgenic mouse strain "MolT-II" carrying a TCR specific for a helper epitope derived from the Moloney murine leukemia virus. Unexpectedly, the characterization of the immune system of MolT-II revealed the TCR-transgenic CD4 T cells to have curtailed functionality and decreased sensitivity to antigenic stimuli.

While CD4 T cells from the similarly TCR-transgenic OT-II mouse model can expand and secrete cytokines upon encountering their cognate epitope, MolT-II CD4 T cells were unable to proliferate or to produce the immune regulatory cytokines IL-2, and TNF, or to upregulate expression of TNF superfamily member CD40L, known to be expressed by activated T cells. Moreover, MolT-II CD4 T cells expressed high levels of both co-inhibitory (PD-1, LAG-3, CTLA-4, TIM-3) and co-stimulatory surface receptors (ICOS, OX40), before and after TCR stimulation. Taken together, these results indicated that MolT-II CD4 T cells are dysfunctional and show clear signs of T cell exhaustion[40–42].

T cell exhaustion is defined as a cell state that arises in response to chronic antigen stimulation, and markers of exhaustion range from limited functionality, to upregulation of inhibitory immune checkpoint molecules and the expression of exhaustion-related transcription factors[1,5,43]. In the context of cancer research, most focus so far has been directed at exhaustion of CD8 T cells, as well as its possible causes and immunotherapeutic interventions to reinstate the tumor killing capacities of CD8 T cells. However, more and more studies are emerging, suggesting that CD4 T cells not only play an invaluable role in different anti-tumor immune responses, but can also experience exhaustion[5,44–46]. CD4 T cells have been shown to be key factors for the clearance of both MHC II-proficient[47–49] and MHC II-deficient tumors[29,50,51]. On the other hand, absence or dysfunction of CD4 T cells can contribute to CD8 T cell exhaustion[52] and lead to tumor progression[53], which is why it is important to also investigate the causes and mechanisms underlying CD4 T cell exhaustion. Similar to CD8 T cell exhaustion, exhausted CD4 T cells have been characterized by low cytokine release and overexpression of inhibitory checkpoint molecules, such as PD-1, LAG-3, CTLA-4, TIM-3, TIGIT, and CD39[46,54–58], but overall there is only a limited number of studies investigating CD4 T cell exhaustion. Interestingly, we found that MolT-II CD4 T cells also express higher levels of co-stimulatory checkpoint molecules like OX40 and ICOS (Supplementary Fig. 2). This exact phenotype has not previously been described, but the co-expression of co-inhibitory and co-stimulatory molecules by dysfunctional CD4 T cells has also been observed in exhausted CD4 T cells during chronic infection, as well as in human and murine cancers[34,59,60]. For example, CD4 T cells co-expressing ICOS, PD-1, LAG-3 and CD39 were found in the microenvironment of MC38 colorectal carcinoma and responded to blockade of PD-1 and LAG-3, and to PD-1 blockade combined with an ICOS agonist[59]. A similar signature of dysfunctional CD4 T cells expressing OX40, ICOS and co-inhibitory checkpoint molecules has been observed in murine glioblastoma models, where cells could be reinvigorated through combining PD-1 blockade with CD40 agonism[52]. Further, a CD4 T cell exhaustion signature caused by sustained antigen exposure in hepatocellular carcinoma patients also includes the expression of OX40[61], and the co-expression of ICOS with several inhibitory checkpoint molecules by CD4 T cells has been identified in immune exhausted human breast cancers[62]. The signatures of exhausted CD4 T cells are likely variable, similarly to CD8 T cells, but more research is required to establish solid criteria and definitions.

Overall, exhausted or dysfunctional CD4 T cells have been found to play a role in different human cancers, where they have been shown to respond to immunotherapy. In human melanoma, tumor-specific CD4 T cells were found to express markers of chronic exhaustion, and upon blockade of PD-L1 and LAG-3 contributed to mediating disease regression[56]. Similarly, dysfunctional CD4 T cells were associated with advanced human hepatocellular carcinoma, while cytokine production could be restored through PD-L1 blockade[63].

A potential cause for the phenotype observed in our model may be the presence of an endogenous antigen, which drives the exhaustion of MolT-II T cells. The reduced number of CD4 T cells in the periphery, the inverted CD8:CD4 T cell ratio and the reduced proportion of double-positive $CD4^+CD8^+$ thymocytes in MolT-II mice all point towards negative selection of TCR-transgenic CD4 T cells[38,64,65]. This phenomenon has previously been described in other TCR-transgenic mouse strains in which TCR ligands are present in the thymus[36,65].

We identified an endogenously expressed antigen with high sequence homology to the cognate MolT-II epitope envH. The envelope protein of the murine retrovirus AKV (AKVenv) only differs from envH at one amino acid position, where instead of a leucine there is a tyrosine. We have found this sequence to be expressed by mTECs in the thymus of MolT-II mice, and show that MolT-II CD4 T cells cross-react with AKVenv, suggesting that the endogenous AKV could play a role for the partial deletion of the MolT-II CD4 T cell compartment[38]. MolT-II thymocytes were normally differentiated but the $CD4^+CD8^+$ double-positive compartment was significantly reduced, as observed in other models for self-reactive thymocytes[66]. Further, as described by Yui K. et al. for self-reactive T cells, the low number of MolT-II CD4 T cells that manage to escape from deletion to the periphery are unresponsive to their cognate epitope but can be activated with a strong TCR stimulus[67]. This phenomenon may be explained through previous reports, which state that negative selection primarily affects high affinity TCRs, leaving only low to moderate affinity TCR T cells to mature and move to the periphery[68].

The presence of TCR ligands in the thymus has also been shown to increase Treg development in some cases[69,70], but we did not observe this in MolT-II mice, which displayed similar levels of Treg cells in the peripheral lymphoid organs as C57BL/6 mice. There may be other, non-T cell factors that could be conducive to an environment further perpetuating the exhausted phenotype we observed. Myeloid-derived suppressor cells and tolerogenic DCs have been shown to inhibit T cell responses through various pathway[71–73].

Another line of evidence for a possible influence of peripheral factors on the phenotype of MolT-II CD4 T cells comes from our experiments using bioluminescence reporter MolT-II*TbiLuc mice. CD4 T cells from these mice constitutively express a luciferase to enable tracking, and express a second luciferase upon activation. To assess the in vivo functionality of MolT-II CD4 T cells, MolT-II*TbiLuc CD4 T cells were transferred to naive C57BL/6 recipient mice, which were then vaccinated. We observed a detectable activation signal from these MolT-II*TbiLuc CD4 T cells after the booster vaccination (Fig. 4C), which could be influenced by the immune environment of the recipient mice. Further experiments are needed to establish whether other cell populations and peripheral factors in MolT-II mice influence the CD4 T cell phenotype.

We were able to partially restore the function of MolT-II CD4 T cells in vivo through immunization with epitope envH and combined checkpoint blockade of PD-1, LAG-3 and CTLA-4. These immune checkpoints have been extensively described in the past two decades as major co-inhibitory regulators in infectious diseases, auto-immunity and cancer. Antibody blockade in the absence of immunization did not have any significant effects on cytokine production and the total number of MolT-II CD4 T cells, indicating that the presence of the endogenous AKVenv epitope is not sufficient as signal 1 to fully activate the CD4 T cells[74,75]. Immunization with envH peptide by itself or in combination with single checkpoint blockade was moderately successful in restoring IL-2 and CD40L production, but did not lead to a significant increase of the total number of CD4 T cells in the lymph nodes and spleens of MolT-II mice. The best activation was achieved when combining envH immunization with simultaneous blockade of PD-1, LAG-3, and CTLA-4. This treatment resulted in significantly elevated production of IL-2 and CD40L, as well as proliferation that led to a 2-3x expansion of the CD4 T cell population. These results reflect observations made by several other investigators, who found that while monotherapies targeting immune checkpoints can restore CD4 T cell function to a degree, combination of different immunotherapies has a superior synergistic effect on T cell activation and tumor survival, which suggests that multiple co-inhibitory pathways are operational in T cell dysfunction[46,52,76,77].

The elevated expression and rapid upregulation of co-inhibitory molecules by MolT-II CD4 T cells makes this model well suited to study how these markers determine the exhausted phenotype in the chronic antigen-presentation environment of tumors, as well as how to use immunomodulatory treatments to rescue the T cell functions in vivo.

Further, we could show that MolT-II CD4 T cells were able to confer protection against tumors in vivo. Transfer of MolT-II cells alone was not sufficient to control RMA tumor outgrowth, but combined with peptide vaccination and a potent adjuvant we were able to

overcome the dysfunctional state of the MolT-II cells. This suggests that in this setting powerful vaccination by itself can be sufficient to reinvigorate exhausted CD4 T cells. In cancer, chronically stimulated CD4 T cells can become dysfunctional and acquire features of exhaustion (reduced cytokine production, altered proliferative capacity and expression of inhibitory receptors), yet they may not be irrevocably terminal and can be functionally reawakened under appropriate stimulatory conditions. Thus, our results are consistent with a model in which vaccination supplies specific antigenic and potent adjuvant signals to restore helper functions of MolT-II cells, amplifying CD8 T cell efficacy and substantially improving tumor control.

The MolT-II model may contribute to identifying the precise parameters that govern CD4 T cell reinvigoration; for example, the role of antigen dose and persistence, the balance between co-stimulatory versus co-inhibitory receptors expression, adjuvant formulation, and the timing of adoptive transfer relative to vaccination. Dissecting these variables will be important to understand when vaccination alone suffices to recover exhausted CD4 help and when additional interventions (e.g., checkpoint blockade or CD40 agonism) are required for optimal reinvigoration of exhausted CD4 T cells to maximize tumor control.

In summary, we established a transgenic mouse model with exhausted CD4 T cells that can regain function through combined synergistic checkpoint immunotherapy. The new mouse model shows features of T cell tolerance, such as T cell depletion, anergy and tuning of activation threshold and is suitable for studying T cell related and non-related mechanisms driving CD4 T cell tolerance in vivo.

Methods

Mice

The TCR-transgenic mouse strain MolT-II was generated at the Leiden University Medical Center ('LUMC', Leiden, Netherlands) on a C57BL/6 background. MolT-II mice express a TCR recognizing peptide Moloney $env_{119\text{-}137}$ in association with I-A^b under control of K^b-promotor IgG enhancer element. The transgenic TCR α and β genes were derived from the Moloney $env_{119\text{-}137}$ specific helper T cell clone 3A12[29]. DNA sequence determination revealed that the TCR's variable gene segments were composed of Vα10.2 and Vβ6. The TCR Vα10.2-J-C and TCR Vβ6-D-J-C regions were amplified by PCR from clone 3A12-derived cDNA with specific primers and cloned into the pHSE3' expression vector[78]. The TCR α- and β-chain gene constructs were linearized and co-injected directly into the pronuclei of fertilized C57BL/6 oocytes. Transgenic founder mice were identified by PCR using specific primers for the Vα-J-C and Vβ-D-J-C regions, and results were confirmed by Southern blot. Transgenic founder mice were bred with C57BL/6 mice and tail blood of transgenic offspring was analyzed by means of PCR and Vβ6 specific monoclonal antibodies to confirm expression of the transgenic TCR on the surface of T cells.

C57BL/6 J mice were obtained from Charles River (l'Arbresle, France; Catalog, 632). TCR-transgenic OT-II mice (originally obtained from Charles River, France; Catalog, 643), TbiLuc reporter mice (dual luciferase transgenic mice for bioluminescence imaging of T cells[39], TbiLuc*MolT-II and TbiLuc-OT-II mice were bred at the animal facility of the LUMC.

Female and male mice were used in all experiments except for the adoptive transfer, sex was not considered as a relevant biological variable in this study. For adoptive transfer experiments, only female mice were used to avoid adverse immune reactions. All animals were aged 8–12 weeks at the beginning of the experiments, and were euthanized by cervical dislocation. All mouse strains were bred and maintained under specific pathogen-free conditions in IVC cages and were co-housed for the duration of experiments, at the LUMC's animal facility (20 °C–22 °C, relative humidity 55%, light cycle with daytime 07:00–18:00 h and 30 min transition periods before and after). All experiments were approved by the animal experiments ethics committee of Leiden University.

Cell lines and peptides

The D1 cell line is a long term growth factor-dependent immature splenic DC line derived from C57BL/6 (H-2^b) mice and was cultured as described elsewhere[79]. For the current study we used the Moloney $env_{119\text{-}137}$ T helper peptide (EPLTSLTPRCNTAWNRLKL, 'envH')[80], AKV $env_{138\text{-}156}$ peptide (EPLTSYTPRCNTAWNRLKL, 'AKVenv')[81], ovalbumin-derived T helper peptide $Ova_{323\text{-}339}$ (ISQAVHAAHAEINEAGR, 'ovaH')[82], and the MuLV gag-leader-derived CTL epitope $gPr80^{gag}{}_{85\text{-}93}$ (CCLCLTVFL, 'gagL')[83]. Further, for in vivo experiments, we used modified versions of envH and AKVenv in which the cysteines at position 10 have been exchanged with α-aminobutyric acid to prevent oxidation (EPLTSLTPRAbuNTAWNRLKL, EPLTSYTPRAbuNTAWNRLKL). All peptides were synthesized at the LUMC (Leiden, Netherlands) on solid-phase using Fmoc chemistry, purified and characterized by mass spectrometry.

Flow cytometry

Spleens, lymph nodes, blood and thymus were harvested from mice and processed to single cell suspensions. For the identification of surface markers, cells were incubated with fluorochrome-conjugated antibodies in PBA (PBS, 0.5% BSA) for 30 min at 4 °C.

For detection of intracellular and intranuclear proteins, cells were fixed, permeabilized and stained using the Cyto-Fast Fix-Perm Buffer Set (Biolegend, USA; Catalog, 426803) or the eBioscience FoxP3/Transcription Factor Staining Buffer Set (Invitrogen, USA; Catalog, 00-5523-00) according to the manufacturer's recommendations. Samples were acquired on LSR-II (with BD FACSDiva software, BD Bioscience, USA) or Aurora 5 L (with SpectroFlo software, Cytek, USA) cytometers, followed by analysis using FlowJo software (FlowJo LLC, USA) and OMIQ (Dotmatics, USA). Details about antibodies used for flow cytometry can be found supplementary table 1. The gating strategy used for identifying different T cell populations is shown in supplementary fig. 4.

CFSE labeling

CFSE labeling of splenocytes was performed as according to kit instructions. Shortly, 25,000 D1 cells were added per well in a 96-well round bottom plate. Antigenic peptides were added to final concentrations of 0.05–5 μM. After incubation at 37 °C for 4 h, cells were washed twice with PBS to remove all remaining antigens from the supernatant. During the last hour of incubation, splenocytes were collected and washed with pre-warmed PBS/BSA (0.1%). For CFSE-labeling, cells were incubated at 37 °C for 10 min with 5 μM CFSE (Thermo Fisher Scientific, USA; Catalog, C34554) at 10×10^6 splenocytes/ml in PBS/BSA (0.1%). The labeling reaction was stopped by adding 10-fold volume of complete medium (IMDM, 10% FCS, 100 U/ml penicillin, 100 μg/ml streptomycin, 2 mM L-glutamine, 25 μM β-Mercaptoethanol). CFSE-labeled cells were spun down and 3×10^5 splenocytes were added per well to the peptide-loaded D1 cells. After 96 h, cells were harvested, washed with PBA, stained and analyzed by flow cytometry.

In vitro and ex vivo (re-)stimulation of T cells

For stimulation of cells with anti-CD3e, 48-well plates were coated with 200 ng/ml or 1000 ng/ml anti-CD3e (clone 145-2C11, BD Biosciences; Catalog, 553057) in PBS for 2 h at 37 °C. Plates were then washed twice with PBS, 1×10^6 total splenocytes in complete medium. were added per well and incubated for 16 h. Cells were then harvested, washed in PBA, stained and analyzed by flow cytometry.

For stimulation of cells with combined anti-CD3e and anti-CD28, 1×10^6 mouse splenocytes were plated per well in 96-well round bottom plates. A mix of 1 mg/ml each of soluble anti-CD3e (clone 145-2C11,

BD Biosciences; Catalog, 553057) and anti-CD28 (clone 37.51, BD Biosciences; Catalog, 553294) was added to the cells. After 1 h of incubation, Brefeldin A was added and cells were incubated for another 4–6 h.

For stimulation of cells with antigenic peptides, 5×10^4 D1 cells were seeded per well in 96-well round bottom plates and incubated with 0.05-10 mM peptide or equivalent volumes of the solvent DMSO for 4–5 h at 37 °C. The plates were then washed twice with PBS to remove any remaining free peptide from the supernatant and 1×10^6 mouse splenocytes were added per well. After 1 h of co-incubation, Brefeldin A was added to prevent cytokine secretion, and the cells were incubated for another 4–6 h at 37 °C, 5% CO_2 before they were washed and stained for flow cytometry. In the case of experiments using mature D1 cells, immature D1 cells were incubated with LPS (4 μg/ml, Sigma-Aldrich, USA) over night at 37 °C prior to co-incubation of 2.5×10^4 mature D1 cells with 7.5×10^5 MolT-II splenocytes and 5 μM peptide, and treatment with Brefeldin A as described above.

Molecular analysis of thymic cells

Isolation of thymic stromal cells was performed as described previously[84]. Thymic lobes were cleaned of fat and connective tissue, cut in little pieces and stirred for 10 min in 15 ml RPMI1640 medium at room temperature to release thymocytes. Tissue fragments were then resuspended in 1 ml medium per sample containing 0.2 mg/ml Collagenase IV (Worthington Biochemical, USA), 10 mM HEPES and 2% FCS. The mixture was slowly stirred for 15 min at 30 °C, released cells removed and fresh enzyme mixture added for a total of 3 incubations. The remaining fragments were digested with a mixture of Collagenase IV and Neutral Protease (0.2 mg/ml each; Worthington Biochemical, USA), 25 μg/ml DNase I (Roche, Switzerland), 10 mM HEPES and 2% FCS in RPMI1640. Five incubations for 25 min at 37 °C were performed. For DC isolation all cells from the collagenase incubations and the first round of collagenase/neutral protease digestion were pooled, washed and rosettes dissociated by 5 min incubation at 37 °C in PBS containing 25 mM EDTA. Cells were stained with anti-CD11c microbeads (Miltenyi Biotec, Germany; Catalog, 130-125-835), run on an AutoMACS (Miltenyi Biotec, Germany) using the "Possel_S" program, blocked with anti-FcR mAb 2.4G2 supernatant including 5 % rat serum and stained with anti-CD11c-PE (clone HL3; BD Biosciences, USA; Catalog, 561044), anti-F4/80-FITC (clone CI:A3-1; Bio-Rad, USA; Catalog, MCA497FA) and propidium iodide (PI). Thymic epithelial cells were enriched by pooling cells from collagenase/neutral protease digestion rounds two to five, followed by staining with anti-CD45 microbeads (Miltenyi Biotec, Germany; Catalog, 130-052-301), run on an AutoMACS using the 'Deplete' program, blocked with anti-FcR mAb 2.4G2 supernatant and stained with anti-Ly51-FITC (clone 6C3; BD Biosciences, USA; Catalog, 562057), anti-CD80-PE (clone 16-10A1; BD Biosciences, USA; Catalog, 561955), anti-EpCAM-Alexa647 (clone G8.8; kindly provided by Dr. B. Kyewski), anti-CD45-PE/Cy5 (clone 30-F11; BD Biosciences, USA; Catalog, 561870) and PI. Dendritic cells were identified as $CD11c^+F4/80^-$. mTECs were identified as $CD45^-$ $Ly51^-EpCAM^+$ and sorted according to their CD80 expression, as $CD80^{hi}$ or $CD80^{lo}$, representing the top and bottom 30% of the population. cTECs were defined as $CD45^-Ly51^+EpCAM^+$. Cell sorting was performed with a FACSAriaI cell sorter (Becton Dickinson, USA).

For quantitative PCR analysis cells were purified by cell sorting and EL-4 thymoma cells grown in culture were treated as published, including two separate DNase I incubation steps. Mela (AKVenv) and beta actin transcripts were amplified with Power SYBR Green Master Mix (Applied Biosystems/Thermo Fisher, USA; Catalog, 4368577) on a GeneAmp 7300 system (Applied Biosystems/Thermo Fisher, USA). Primers used for the amplification were kindly provided by Dr. B. Kyewski (produced at the oligonucleotide synthesis facility of the German Cancer Research Center, Germany) and can be found in supplementary table 2.

In vivo T cell transfer. For in vivo bioluminescence imaging of the localization and activation of CD4 T cells, TbiLuc mice were crossed to MolT-II and OT-II mice, to obtain TbiLuc*MolT-II and TbiLuc*OT-II mice. Spleens of TbiLuc*MolT-II and TbiLuc*OT-II mice were collected and processed to single cell suspensions, followed by enrichment of CD4 T cells from the splenocytes using a Mouse CD4 T Lymphocyte Enrichment Set (BD Bioscience, USA; Catalog, 558131). 2×10^6 enriched CD4 T cells were transferred into C57BL/6 mice through intravenous injection in 200 μl PBS (day 0). The recipient mice were then immunized on day 1 and 11 with 5 nmol peptide envH + 5 nmol CpG (TbiLuc*MolT-II), 5 nmol peptide ovaH + 5 nmol CpG (TbiLuc*OT-II) or left unvaccinated.

In vivo bioluminescence imaging of T cells

Bioluminescence imaging of transferred TbiLuc*MolT-II or TbiLuc*OT-II CD4 T cells occurred under isoflurane anesthesia using an IVIS Spectrum Imager (PerkinElmer, Waltham, MA, USA) with Living Image software (Revvity, USA). Mice were imaged every 2-4 days over a period of 4 weeks. To image the localization of T cells, mice were injected subcutaneously (s.c.) with 150 mg/kg D-luciferin imaged after 10 min at the peak of emission, using the open and 560 nm filters with auto exposure. To image the activation of CD4 T cells, the animals were injected s.c. with 7.6 mg/kg CycLuc1 and imaged after 8 min using the open and 620 nm filters with auto exposure.

Bioluminescence signals were quantified using fixed-sized, fixed-position regions of interest (ROIs) and corrected for background signals with Aura Imaging Software (Spectral Instruments Imaging, USA).

In vivo antibody blocking

MolT-II mice were injected intraperitoneally with 10 mg/kg Rat anti-mouse PD-L1 (MIH5, kindly provided by Dr. R. Arens (LUMC, Leiden, Netherlands)), Rat anti-mouse LAG-3 (clone C9B7W, BioXCell; Catalog, BE0174) and/or Syrian hamster anti-mouse CTLA-4 (clone 9H10, BioXCell; Catalog, BE0131) on days 0, 2 and 4. Control Rat anti-β-galactosidase (clone GL113, kindly provided by Dr. R. Arens) was also injected at a dose of 10 mg/kg. On day 1, mice were immunized with 10 nmol envH peptide mixed with 5 nmol CpG or an equivalent volume of the solvent in PBS. On day 6, spleens and draining lymph nodes were collected and processed into single cell suspensions for intracellular cytokine staining and flow cytometry.

In vivo tumor experiments

Tumor experiments were performed with four groups of C57BL/6 mice. The control group (n = 16) was s.c. (subcutaneously) injected with a 1:1 IFA:PBS mixture, the 'MolT-II' group (n = 8) also received 1:1 IFA:PBS and an intravenous (i.v.) transfer of 1×10^7 MolT-II cells from the spleens and lymph nodes of naïve MolT-II mice. The 'envH + gagL' group (n = 16) was s.c. vaccinated with 20 nmol gagL peptide and 20 nmol envH peptide emulsified in 1:1 IFA:PBS, the 'MolT-II + envH + gagL' group (n = 15) received the same vaccination as well as i.v. transfer of 1×10^7 MolT-II cells. All animals were inoculated with 2000 RMA cells in the right flank, followed by an observation period of 60 days, in which the growth of tumor lesions was monitored. Mice were euthanized by cervical dislocation when tumors exceeded the maximum size allowed by the ethics board of 1000 mm^3 or became necrotic. The maximum tumor size was not exceeded. Tumors were measured using calipers and volume was calculated using the equation volume = (length x width x height) / 2.

Statistics

Statistical analysis was performed using GraphPad Prism 10.2.3 (GraphPad Software, Boston, MA,USA). Data are shown as mean ± SD or mean ± SEM, depending on the experiment. Differences were considered statistically significant at $p < 0.05$. Multiplicity-adjusted P

values are depicted in the figures as follows: *P ≤ 0.05, **P ≤ 0.01, ***P ≤ 0.001, and ****P ≤ 0.0001.

Study approval

All animal experiments were performed in accordance with the guidelines of the Dutch Animal Ethics Committee and the recommendations set by the LUMC and by the Dutch Experiments on Animals Act. All animal experience were approved by the Animal Welfare Body of LUMC (permit AVD11600202013796).

Reporting summary

Further information on research design is available in the Nature Portfolio Reporting Summary linked to this article.

Data availability

All data are included in the Supplementary Information or available from the authors, as are unique reagents used in this article. The raw numbers for charts and graphs are available in the Source Data file whenever possible. Source data are provided with this paper.

References

1. Jiang, Y. et al. T-cell exhaustion in the tumor microenvironment. *Cell Death Dis.* **6**, e1792 (2015).
2. Chow, A. et al. Clinical implications of T cell exhaustion for cancer immunotherapy. *Nat. Rev. Clin. Oncol.* **19**, 775–790 (2022).
3. Brunell, A. E. et al. Exhausted T cells hijacking the cancer-immunity cycle: assets and liabilities. *Front Immunol.* **14**, 1151632 (2023).
4. Saeidi, A. et al. T-cell exhaustion in chronic infections: reversing the state of exhaustion and reinvigorating optimal protective immune responses. *Front Immunol.* **9**, 2569 (2018).
5. Miggelbrink, A. M. et al. CD4 T-cell exhaustion: does it exist and what are its roles in cancer? *Clin. Cancer Res.* **27**, 5742–5752 (2021).
6. de Graaf, J. F. et al. Neoantigen-specific T cell help outperforms non-specific help in multi-antigen DNA vaccination against cancer. *Mol. Ther. Oncol.* **32**, 200835 (2024).
7. Facciabene, A. et al. Tumour hypoxia promotes tolerance and angiogenesis via CCL28 and T(reg) cells. *Nature* **475**, 226–230 (2011).
8. Chaudhary, B. & Elkord, E. Regulatory T cells in the tumor microenvironment and cancer progression: role and therapeutic targeting. *Vaccines* **4**, 28 (2016).
9. Oh, D. Y. et al. Intratumoral CD4(+) T cells mediate anti-tumor cytotoxicity in human bladder cancer. *Cell* **181**, 1612–1625 (2020).
10. Takeuchi, A. & Saito, T. CD4 CTL, a cytotoxic subset of CD4(+) T cells, their differentiation and function. *Front. Immunol.* **8**, 194 (2017).
11. Bogen, B. et al. CD4(+) T cells indirectly kill tumor cells via induction of cytotoxic macrophages in mouse models. *Cancer Immunol. Immunother.* **68**, 1865–1873 (2019).
12. Kruse, B. et al. CD4(+) T cell-induced inflammatory cell death controls immune-evasive tumours. *Nature* **618**, 1033–1040 (2023).
13. Veatch, J. R. et al. Neoantigen-specific CD4(+) T cells in human melanoma have diverse differentiation states and correlate with CD8(+) T cell, macrophage, and B cell function. *Cancer Cell* **40**, 393–409 (2022).
14. Luca, B. A. et al. Atlas of clinically distinct cell states and ecosystems across human solid tumors. *Cell* **184**, 5482–5496 (2021).
15. Lei, X. et al. CD4(+) T cells produce IFN-I to license cDC1s for induction of cytotoxic T-cell activity in human tumors. *Cell Mol. Immunol.* **21**, 374–92 (2024).
16. Thorsson, V. et al. The immune landscape of cancer. *Immunity* **48**, 812–830 (2018).
17. Collier, J. L. et al. Not-so-opposite ends of the spectrum: CD8(+) T cell dysfunction across chronic infection, cancer and autoimmunity. *Nat. Immunol.* **22**, 809–19 (2021).
18. Sowell, R. T. & Kaech, S. M. Probing the diversity of T cell dysfunction in cancer. *Cell* **166**, 1362–1364 (2016).
19. Zhao, Y. et al. Exhaustion and senescence: two crucial dysfunctional states of T cells in the tumor microenvironment. *Cell Mol. Immunol.* **17**, 27–35 (2020).
20. Tonnerre, P. et al. Differentiation of exhausted CD8(+) T cells after termination of chronic antigen stimulation stops short of achieving functional T cell memory. *Nat. Immunol.* **22**, 1030–1041 (2021).
21. van der Heide, V. et al. Advancing beyond the twists and turns of T cell exhaustion in cancer. *Sci. Transl. Med.* **14**, eabo4997 (2022).
22. Dong, Y. et al. CD4(+) T cell exhaustion revealed by high PD-1 and LAG-3 expression and the loss of helper T cell function in chronic hepatitis B. *BMC Immunol.* **20**, 27 (2019).
23. Lee, J. et al. Reinvigorating exhausted T cells by blockade of the PD-1 pathway. *Immunopathol. Dis. Ther.* **6**, 7–17 (2015).
24. Sobhani N, et al. CTLA-4 in regulatory T Cells for cancer immunotherapy. *Cancers* **13**, 1440 (2021).
25. Huo, J. L. et al. The promising immune checkpoint LAG-3 in cancer immunotherapy: from basic research to clinical application. *Front. Immunol.* **13**, 956090 (2022).
26. Das, S. & Johnson, D. B. Immune-related adverse events and anti-tumor efficacy of immune checkpoint inhibitors. *J. Immunother. Cancer* **7**, 306 (2019).
27. Terranova-Barberio, M. et al. Exhausted T cell signature predicts immunotherapy response in ER-positive breast cancer. *Nat. Commun.* **11**, 3584 (2020).
28. Cuypers, H. T. et al. Murine leukemia virus-induced T-cell lymphomagenesis: integration of proviruses in a distinct chromosomal region. *Cell* **37**, 141–150 (1984).
29. Ossendorp, F. et al. Specific T helper cell requirement for optimal induction of cytotoxic T lymphocytes against major histocompatibility complex class II negative tumors. *J. Exp. Med.* **187**, 693–702 (1998).
30. van Hall, T. et al. Identification of a novel tumor-specific CTL epitope presented by RMA, EL-4, and MBL-2 lymphomas reveals their common origin. *J. Immunol.* **165**, 869–877 (2000).
31. Schepers, K. et al. Differential kinetics of antigen-specific CD4+ and CD8+ T cell responses in the regression of retrovirus-induced sarcomas. *J. Immunol.* **169**, 3191–3199 (2002).
32. Johnson, D. K. et al. CD4 inhibits helper T cell activation at lower affinity threshold for full-length T cell receptors than single chain signaling constructs. *Front. Immunol.* **11**, 561889 (2020).
33. Au-Yeung, B. B. et al. A sharp T-cell antigen receptor signaling threshold for T-cell proliferation. *Proc. Natl. Acad. Sci. USA* **111**, E3679–E3688 (2014).
34. Crawford, A. et al. Molecular and transcriptional basis of CD4(+) T cell dysfunction during chronic infection. *Immunity* **40**, 289–302 (2014).
35. Baaten, B. J. et al. Regulation of antigen-experienced T cells: lessons from the quintessential memory marker CD44. *Front Immunol.* **3**, 23 (2012).
36. Caton, A. J. et al. Immune recognition of influenza hemagglutinin as a viral and a neo-self-antigen. *Immunol. Res.* **17**, 23–32 (1998).
37. von Boehmer, H. Developmental biology of T cells in T cell-receptor transgenic mice. *Annu Rev. Immunol.* **8**, 531–556 (1990).
38. Klein, L. et al. Positive and negative selection of the T cell repertoire: what thymocytes see (and don't see). *Nat. Rev. Immunol.* **14**, 377–391 (2014).
39. Kleinovink, J. W. et al. A dual-color bioluminescence reporter mouse for simultaneous in vivo imaging of T cell localization and function. *Front. Immunol.* **9**, 3097 (2018).
40. Yi, J. S. et al. T-cell exhaustion: characteristics, causes and conversion. *Immunology* **129**, 474–481 (2010).
41. Thommen, D. S. & Schumacher, T. N. T cell dysfunction in cancer. *Cancer Cell* **33**, 547–562 (2018).

42. Hashimoto, M. et al. CD8 T cell exhaustion in chronic infection and cancer: opportunities for interventions. *Annu. Rev. Med.* **69**, 301–318 (2018).
43. Blank, C. U. et al. Defining 'T cell exhaustion. *Nat. Rev. Immunol.* **19**, 665–674 (2019).
44. Nagasaki, J. & Togashi, Y. A variety of 'exhausted' T cells in the tumor microenvironment. *Int. Immunol.* **34**, 563–570 (2022).
45. Tracy, S. I. et al. Combining nilotinib and PD-L1 blockade reverses CD4+ T-cell dysfunction and prevents relapse in acute B-cell leukemia. *Blood* **140**, 335–348 (2022).
46. Yuan, L. et al. Tumor-infiltrating CD4(+) T cells in patients with gastric cancer. *Cancer Cell Int.* **17**, 114 (2017).
47. Haabeth, O. A. W. et al. CD4(+) T-cell-mediated rejection of MHC class II-positive tumor cells is dependent on antigen secretion and indirect presentation on host APCs. *Cancer Res.* **78**, 4573–4585 (2018).
48. Quezada, S. A. et al. Tumor-reactive CD4(+) T cells develop cytotoxic activity and eradicate large established melanoma after transfer into lymphopenic hosts. *J. Exp. Med.* **207**, 637–650 (2010).
49. Xie, Y. et al. Naive tumor-specific CD4(+) T cells differentiated in vivo eradicate established melanoma. *J. Exp. Med.* **207**, 651–667 (2010).
50. Perez-Diez, A. et al. CD4 cells can be more efficient at tumor rejection than CD8 cells. *Blood* **109**, 5346–5354 (2007).
51. Brightman, S. E. et al. Neoantigen-specific stem cell memory-like CD4(+) T cells mediate CD8(+) T cell-dependent immunotherapy of MHC class II-negative solid tumors. *Nat. Immunol.* **24**, 1345–1357 (2023).
52. Khan SM, et al. Impact of CD4 T cells on intratumoral CD8 T-cell exhaustion and responsiveness to PD-1 blockade therapy in mouse brain tumors. *J. Immunother. Cancer* **10**, e005293 (2022).
53. Yamada K, et al. Reduced number and immune dysfunction of CD4+ T cells in obesity accelerate colorectal cancer progression. *Cells* **12**, 86 (2022).
54. Balanca, C. C. et al. Dual relief of t-lymphocyte proliferation and effector function underlies response to PD-1 blockade in epithelial malignancies. *Cancer Immunol. Res.* **8**, 869–882 (2020).
55. Fu, J. et al. CD4(+) T cell exhaustion leads to adoptive transfer therapy failure which can be prevented by immune checkpoint blockade. *Am. J. Cancer Res* **10**, 4234–4250 (2020).
56. Goding, S. R. et al. Restoring immune function of tumor-specific CD4+ T cells during recurrence of melanoma. *J. Immunol.* **190**, 4899–909 (2013).
57. Malandro, N. et al. Clonal abundance of tumor-specific CD4(+) T cells potentiates efficacy and alters susceptibility to exhaustion. *Immunity* **44**, 179–193 (2016).
58. Balanca CC, et al. PD-1 blockade restores helper activity of tumor-infiltrating, exhausted PD-1hiCD39+ CD4 T cells. *JCI Insight.* **6**, e142513 (2021).
59. Beyrend, G. et al. PD-L1 blockade engages tumor-infiltrating lymphocytes to co-express targetable activating and inhibitory receptors. *J. Immunother. Cancer* **7**, 217 (2019).
60. Ozkazanc, D. et al. Functional exhaustion of CD4(+) T cells induced by co-stimulatory signals from myeloid leukaemia cells. *Immunology* **149**, 460–471 (2016).
61. Chi, H. et al. T-cell exhaustion signatures characterize the immune landscape and predict HCC prognosis via integrating single-cell RNA-seq and bulk RNA-sequencing. *Front. Immunol.* **14**, 1137025 (2023).
62. Tietscher, S. et al. A comprehensive single-cell map of T cell exhaustion-associated immune environments in human breast cancer. *Nat. Commun.* **14**, 98 (2023).
63. Zhao, Q. et al. BTLA identifies dysfunctional PD-1-expressing CD4(+) T cells in human hepatocellular carcinoma. *Oncoimmunology* **5**, e1254855 (2016).
64. Bains, I. et al. Models of self-peptide sampling by developing T cells identify candidate mechanisms of thymic selection. *PLoS Comput. Biol.* **9**, e1003102 (2013).
65. Madley, R. et al. Negative selection of human T cells recognizing a naturally-expressed tissue-restricted antigen in the human thymus. *J. Transl. Autoimmun.* **3**, 100061 (2020).
66. Kovalovsky, D. et al. A novel TCR transgenic model reveals that negative selection involves an immediate, Bim-dependent pathway and a delayed, Bim-independent pathway. *PLoS One* **5**, e8675 (2010).
67. Yui, K. et al. Self-reactive T cells can escape clonal deletion in T-cell receptor V beta 8.1 transgenic mice. *Proc. Natl. Acad. Sci. USA* **87**, 7135–7139 (1990).
68. Zinzow-Kramer, W. M. et al. Adaptation by naive CD4(+) T cells to self-antigen-dependent TCR signaling induces functional heterogeneity and tolerance. *Proc. Natl. Acad. Sci. USA* **116**, 15160–15169 (2019).
69. Killebrew, J. R. et al. A self-reactive TCR drives the development of Foxp3+ regulatory T cells that prevent autoimmune disease. *J. Immunol.* **187**, 861–869 (2011).
70. Lee, T. et al. Ectopic expression of self-antigen drives regulatory T cell development and not deletion of autoimmune T cells. *J. Immunol.* **199**, 2270–2278 (2017).
71. Feng, S. et al. Myeloid-derived suppressor cells inhibit T cell activation through nitrating LCK in mouse cancers. *Proc. Natl. Acad. Sci. USA* **115**, 10094–10099 (2018).
72. Ness, S. et al. Regulatory dendritic cells, T cell tolerance, and dendritic cell therapy for immunologic disease. *Front. Immunol.* **12**, 633436 (2021).
73. van Wigcheren, G. F. et al. Myeloid-derived suppressor cells and tolerogenic dendritic cells are distinctively induced by PI3K and Wnt signaling pathways. *J. Biol. Chem.* **299**, 105276 (2023).
74. Bretscher, P. A. A two-step, two-signal model for the primary activation of precursor helper T cells. *Proc. Natl. Acad. Sci. USA* **96**, 185–190 (1999).
75. Sade-Feldman, M. et al. Resistance to checkpoint blockade therapy through inactivation of antigen presentation. *Nat. Commun.* **8**, 1136 (2017).
76. Butterfield, L. H. & Najjar, Y. G. Immunotherapy combination approaches: mechanisms, biomarkers and clinical observations. *Nat. Rev. Immunol.* **24**, 399–416 (2024).
77. Guo, M. et al. Molecular, metabolic, and functional CD4 T cell paralysis in the lymph node impedes tumor control. *Cell Rep.* **42**, 113047 (2023).
78. Pircher, H. et al. Tolerance induction in double specific T-cell receptor transgenic mice varies with antigen. *Nature* **342**, 559–561 (1989).
79. Winzler, C. et al. Maturation stages of mouse dendritic cells in growth factor-dependent long-term cultures. *J. Exp. Med.* **185**, 317–328 (1997).
80. Iwashiro, M. et al. Multiplicity of virus-encoded helper T-cell epitopes expressed on FBL-3 tumor cells. *J. Virol.* **67**, 4533–4542 (1993).
81. Lenz, J. et al. Nucleotide sequence of the AKV ENV gene. *J. Virol.* **42**, 519–529 (1982).
82. Michalek, M. T. et al. Two genetically identical antigen-presenting cell clones display heterogeneity in antigen processing. *Proc. Natl. Acad. Sci. USA* **86**, 3316–20 (1989).
83. Chen, W. et al. Identification of a gag-encoded cytotoxic T-lymphocyte epitope from FBL-3 leukemia shared by friend, moloney, and rauscher murine leukemia virus-induced tumors. *J. Virol.* **70**, 7773–7782 (1996).
84. Derbinski, J. et al. Promiscuous gene expression in thymic epithelial cells is regulated at multiple levels. *J. Exp. Med.* **202**, 33–45 (2005).

Acknowledgements
C.M.B. was supported by a Dr. Mildred Scheel Grant from the German Cancer Aid (Deutsche Krebshilfe, Bonn, Germany). This work and the generation of the TCR-transgenic MolT-II mouse strain were supported by the Dutch Cancer Society (project RUL 2001-2463, F.O.) and the German Cancer Research Center (DKFZ) Heidelberg, Germany. The authors thank Dr. Sjef Verbeek for help with the generation of the TCR-transgenic mouse and Dr. Ramon Arens for providing antibodies for immunotherapy. Further, the authors want to express their gratitude to Bruno Kyewski and Jens Derbinski for their assistance with analyzing the thymic expression of AKVenv.

Author contributions
F.O., M.G.M.C., S.V., and C.J.M.M. were responsible for the design and generation of the MolT-II mouse model. F.S.S., C.M.B., M.G.M.C., T.A., and H.J.T.v.Z. were responsible for performing experiments and data acquisition. F.S.S., C.M.B., C.J.M.M., M.G.M.C., T.A., and F.O. interpreted the data. F.S.S. wrote the manuscript. F.O. and T.A. supervised the project.

Competing interests
The authors declare no competing interests.

Additional information
Supplementary information The online version contains supplementary material available at https://doi.org/10.1038/s41467-025-67588-6.

Correspondence and requests for materials should be addressed to Ferry Ossendorp.

Peer review information *Nature Communications* thanks Dong-il Kwon and the other anonymous reviewer(s) for their contribution to the peer review of this work. A peer review file is available.